IJREAT International Journal of Research in Engineering & Advanced Technology, Volume 3, Issue 1, Feb-Mar, 2015
ISSN: 2320 – 8791 (Impact Factor: 1.479)
www.ijreat.org

2-D Depth Averaged Modelling for Curvilinear Braided Stretch of River Brahmaputra in India

M. P. Akhtar[1], Nayan Sharma[2], C.S.P.Ojha[3]

[1]Water Resources Department, Patna, Patna-800015, India

[2]Department ofWRD&M, Indian Institute of TechnologyRoorkee, Roorkee-247 667, INDIA

[3]Civil Engineering Department, Indian Institute of Technology,Roorkee, Roorkee-247 667, India

Abstract

Flow simulation in Brahmaputra River is rather extremely difficult task due to the inherent complexities in channel process. In this study, the depth averaged 2-D model is applied to simulate the flow field in the 100 km long reach between Guwahati and Jogighopa in the Brahmaputra River in Assam flood plain in India. The model solves 2-D depth averaged equations with modified flow dispersion stress tensor as additional source/sink terms. Dispersion Stress terms take into account the effect of secondary flow variation arisen due to integration of the product of discrepancy between depth averaged velocity and the true velocity distributions. The model uses finite volume method with SIMPLEC algorithm and Rhie and Chow's momentum interpolation technique on curvilinear, non-staggered grid. Wetting and drying process was included into the model for possible simulation of braiding process of the river. The simulated discharges and water elevations are in reasonably good agreement with the measures data.

Keywords: *Depth Averaged Two Dimensional Model, Finite Volume Method, Boundary Fitted Coordinates, Braiding and Secondary flow.*

1. Introduction

The Brahmaputra River, termed as a moving ocean[1], is a snow-fed large Trans-Himalayan river. Large variations in width, gradient, discharge and channel pattern occur throughout its course. The river basin of the Brahmaputra is bounded on the north by the Kailas and Nyen- Chen-TanghIa ranges of mountains; on the east by the Salween river basin and the Patkai range running along the Indo-Myanmar border; on the south by the Nepal Himalayas, the Naga and Barail ranges and the Meghalaya Plateau; and on the west by the Ganga river basin [2]. The Brahmaputra river system is the largest in South Asia draining a catchment area of 580000 sq.km and flows through Tibet (China), India, Bhutan and Bangladesh. This mighty river runs for 2880 kms through China, India and Bangladesh. The problems of flood, erosion and drainage congestion in the Brahmaputra basin are gigantic. The river has braided channel in most of its course in the alluvial plains of Assam. Bank oscillation also causes shifting of outfalls of its tributaries bringing newer areas under waters. At the exit of the gorge the slope of the river is only 0.27 m/km. At the head of the valley near Dibrugarh the river has a gradient of 0.09-0.17 m/km, which is further reduced to about 0.1 m/km near Pandu. The mighty Brahmaputra rolls down the Assam valley from east to west for a distance of 640 km up to Bangladesh border. The location map of Brahamputra River in India is shown in Fig. 1. Figure 2 depicts a typical cross section in Brahmaputra River. The distance between two banks is about 20 km in many reaches. The whole cross section includes main channel, low flood plains, and high flood plains.

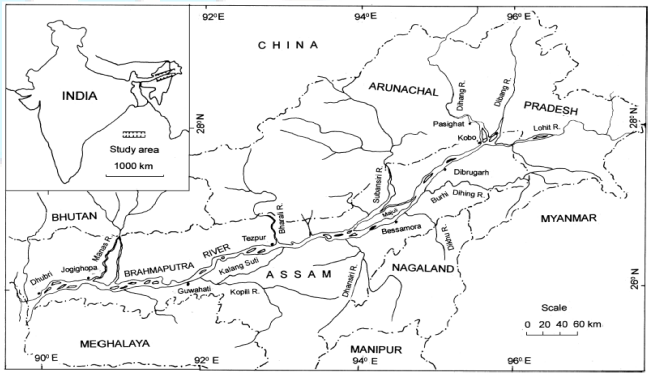

Fig.1Location map of the Brahmaputra River in Assam, India [2]

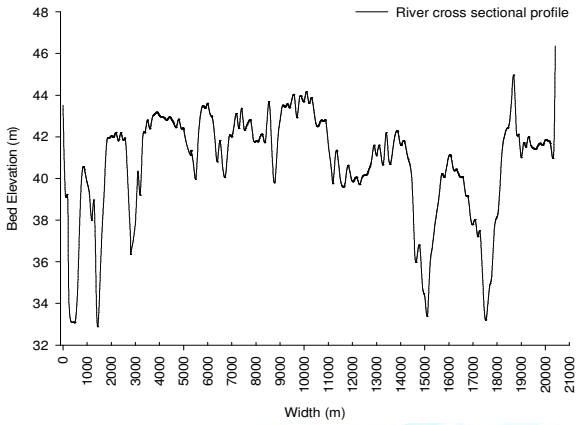

Fig.2Typical cross section in Brahmaputra River for 1997

2. 2-D or 3-D mathematical modelling for braided rivers

Rivers meanders and plan-form have strong circulation associated with bed topography with water surface gradients and associated pressures. Indicating flow field has both topographic as well as bottom shear stress terms. It implies application of *CFD* with topographic 1-D modeling fails when there is significant flow variability in either the vertical or the cross stream direction commonly associated with secondary circulation due to flow curvature or turbulence. For predicting the magnitude and timing of an out of bank flow, 1-D models are adequate. However, where the interest within reach flows with variability is concerned; one needs a 2-D if not a 3-D, treatment [3].

Secondary currents, occur in the plane normal to the axis of the primary flow, they originate from interactions between the primary flow and gross channel features [4]. Secondary transverse flow results from the imbalance between transverse water surface gradient force and centrifugal forces over the depth due to vertical variation of the primary flow velocity [5]. In braided rivers most channel changes are associated with changes in bed morphology, which occur at high discharges when observation is very difficult[6]. Any mention of secondary currents in braided systems has been restricted to areas of channel confluence, and the effect of secondary currents in bifurcations and around braid bars has been largely neglected [7].A number of attempts have been done to simulate the realistic flow field including transverse components in complex geometry like bends, curves[5] [8] [9] [10]. However, assessment of flow-field in braided river with 'secondary flow correction' in complex geometry is hardly found in literature.

The Assam section of the Brahmaputra River is in fact, highly braided and characterized by the presence of numerous lateral as well as mid channel bars and islands [11]. Due to these facts, the research on Brahmaputra River in the past mostly relied on field investigation and physical modelling. Only after 1980s, numerical modelling, especially 1-D modelling has been gradually applied in flow simulation and sediment prediction in Brahmaputra River[12]. Yet successful implementation of 2-D depth averaged modelling in Brahmaputra River Reaches in Assam Flood Plains is hardly found in literature due to its highly complex topography and difficulty in reproduction of geometric data mathematically.

The objective of the present study is to develop and test a numerical 2-D depth averaged model by applying it to 100 km of braided stretch of River Brahmaputra in Assam flood plain of Indian Territory. The model solves 2-D depth averaged equations with modified flow dispersion stress tensor as additional source/sink terms. Dispersion Stress terms take into account the effect of secondary flow variation arisen due to integration of the product of discrepancy between depth averaged velocity and the true velocity distributions. The model uses finite volume method with SIMPLEC algorithm and Rhie and Chow's [13] momentum interpolation technique on curvilinear, non-staggered grid. Wetting and drying process[14] was included into the model for possible simulation of braiding process of the River.

3. Governing equations

The governing equations are RANS equations with depth averaged approximation of continuity and momentum equation (Eqs (1), (2) and (3)) in Cartesian coordinate system [15].

$$\frac{\partial \rho h}{\partial t}+\frac{\partial}{\partial x}\left(\rho h U_x\right)+\frac{\partial}{\partial y}\left(\rho h U_y\right)=0 \quad (1)$$

$$\frac{\partial}{\partial t}\left(\rho h U\right)+\frac{\partial}{\partial x}\left(\rho h U_x{}^2\right)+\frac{\partial D_{xx}}{\partial x}+\frac{\partial}{\partial y}\left(\rho h U_x U_y\right)+\frac{\partial D_{xy}}{\partial y}$$

$$=-\rho g h\frac{\partial H}{\partial x}-C_d \rho U_x\sqrt{U_x{}^2+U_y{}^2}+\rho h \nu_t\left(\frac{\partial^2 U_x}{\partial x^2}+\frac{\partial^2 U_x}{\partial y^2}\right) \quad (2)$$

$$\frac{\partial}{\partial t}\left(\rho h U_y\right)+\frac{\partial}{\partial x}\left(\rho h U_x U_y\right)+\frac{\partial D_{xy}}{\partial x}+\frac{\partial}{\partial y}\left(\rho h U_y^{\,2}\right)+\frac{\partial D_{yy}}{\partial y}$$

$$=-\rho g h\frac{\partial H}{\partial y}-C_d\rho U_y\sqrt{U_x^{\,2}+U_y^{\,2}}+h\rho\nu_t\left(\frac{\partial^2 U_y}{\partial x^2}+\frac{\partial^2 U_y}{\partial y^2}\right) \quad (3)$$

where U_x and U_y = depth-averaged velocity components in x and y directions; t=time; ρ=density of water (kg/m^3); H=water surface elevation; h=depth of the flow; g=acceleration of gravity; C_d=frictional stress coefficient (for friction shear stress at the bottom in x and y directions); and equals $n^2\rho g / h^{\frac{1}{3}}$ with n=Manning's coefficient; ν_t =eddy viscosity;

3.1 Transformed governing equations with dispersion stress tensor

Components of dispersion stress terms in Cartesian coordinate which can be included in momentum transport equations are D_{xx}, D_{xy} and D_{yy}. These terms can be expressed as follows[16];

$$D_{xx}=\int_{z_0}^{h+z_0}\rho\left(u_x-U_x\right)^2 dz$$

$$D_{xy}=\int_{z_0}^{h+z_0}\rho\left(u_x-U_x\right)\left(u_y-U_y\right)dz$$

$$D_{yy}=\int_{z_0}^{h+z_0}\rho\left(u_y-U_y\right)^2 dz \quad (4)$$

wherez_0=zero velocity level.

For open channel free surface gravity flow, cohesive terms are non-significant and can be neglected. The depth averaged parabolic eddy viscosity model (Zero equation model) is adopted for the turbulence term. The depth averaged eddy viscosity is computed as (Eq. (5)) 17] [18].

$$\nu_t=\frac{1}{6}\kappa U_* h \quad (5)$$

Where κ=Von Karman' coefficient and U_*(Shear velocity) $=\left[C_d\left(U_x^{\,2}+U_y^{\,2}\right)\right]^{1/2}$

The transformed depth averaged governing equations in generalized curvilinear coordinate system (ξ, η, τ) for continuity and momentum equation (Eqs(6),(7) and (8)) are derived as follows.

$$\frac{\partial}{\partial\tau}(\rho hJ)+\frac{\partial}{\partial\xi}(\rho hJ\,\hat{u}_\xi)+\frac{\partial}{\partial\eta}(\rho hJ\,\hat{u}_\eta)=0 \quad (6)$$

$$\frac{\partial}{\partial\tau}(\rho hJU_x)+\frac{\partial}{\partial\xi}\left[\rho hJ\hat{u}_\xi U_x\right]+\frac{\partial}{\partial\eta}\left[\rho hJ\hat{u}_\eta U_x\right]-\rho hJ\nu_t\left(\alpha_{11}\frac{\partial^2 U_x}{\partial\xi^2}+\alpha_{22}\frac{\partial^2 U_x}{\partial\eta^2}\right)$$

$$=-\rho ghJ\left(\xi_x\frac{\partial H}{\partial\xi}+\eta_x\frac{\partial H}{\partial\eta}\right)-C_d\rho J(U_x)\sqrt{(U_x)^2+(U_y)^2} \quad (7)$$

$$+\rho hJ\nu_t\alpha_{12}\frac{\partial^2 U_x}{\partial\xi\partial\eta}-\left(\xi_x\frac{\partial D_{xx}}{\partial\xi}+\eta_x\frac{\partial D_{xx}}{\partial\eta}+\xi_y\frac{\partial D_{xy}}{\partial\xi}+\eta_y\frac{\partial D_{xy}}{\partial\eta}\right)$$

$$\frac{\partial}{\partial\tau}(\rho hJU_y)+\frac{\partial}{\partial\xi}\left[\rho hJ\hat{u}_\xi U_y\right]+\frac{\partial}{\partial\eta}\left[\rho hJ\hat{u}_\eta U_y\right]-\rho hJ\nu_t\left(\alpha_{11}\frac{\partial^2 U_y}{\partial\xi^2}+\alpha_{22}\frac{\partial^2 U_y}{\partial\eta^2}\right)=$$

$$-\rho ghJ\left(\xi_y\frac{\partial H}{\partial\xi}+\eta_y\frac{\partial H}{\partial\eta}\right)-C_d\rho J(U_y)\sqrt{(U_x)^2+(U_y)^2} \quad (8)$$

$$+\rho hJ\nu_t\left(\alpha_{12}\frac{\partial^2 U_y}{\partial\xi\partial\eta}\right)-\left(\xi_x\frac{\partial D_{xy}}{\partial\xi}+\eta_x\frac{\partial D_{xy}}{\partial\eta}+\xi_y\frac{\partial D_{yy}}{\partial\xi}+\eta_y\frac{\partial D_{yy}}{\partial\eta}\right)$$

where, $\xi_x=\partial\xi/\partial x$, $\eta_x=\partial\eta/\partial x$, $\xi_y=\partial\xi/\partial y$, $\eta_y=\partial\eta/\partial y$

$\alpha_{11}=\xi_x^{\,2}+\xi_y^{\,2}$, $\alpha_{22}=\eta_x^{\,2}+\eta_y^{\,2}$,

$\alpha_{12}=2(\xi_x\eta_y+\xi_y\eta_x)$, $J=x_\xi y_\eta-x_\eta y_\xi$,

In Eqs(6) to(8); $\hat{u}_m$ (m=ξ, η) are the velocity components in the curvilinear coordinate (ξ,η,τ) which relate to U_x, $U_y$as

$$\begin{pmatrix}\hat{u}_\xi\\ \hat{u}_\eta\end{pmatrix}=\begin{pmatrix}\xi_x & \xi_y\\ \eta_x & \eta_y\end{pmatrix}\begin{pmatrix}U_x\\ U_y\end{pmatrix} \quad (9)$$

The relation between depth averaged velocities in curvilinear coordinates and Cartesian coordinate can be given as Duan[16]

$$U_x=U_s\cos\theta_s+U_n\cos\theta_n$$

$$U_y=U_s\sin\theta_s+U_n\sin\theta_n \quad (10)$$

In Eq. (10), $\theta_s$and θ_n are angles between stream-wise, transverse directions pointing outward and positive x-axis respectively. Similarly the dispersion terms in Cartesian coordinates can be related to that in curvilinear coordinates as follows [16]

$$D_{xx}=D_{xx}^c\cos^2\theta_s+2D_{xy}^c\cos\theta_s\cos\theta_n+D_{yy}^c\cos^2\theta_n \quad (11)$$

$$D_{yy}=D_{xx}^c\sin^2\theta_s+2D_{xy}^c\sin\theta_s\sin\theta_n+D_{yy}^c\sin^2\theta_n$$

$$D_{xy}=D_{xx}^c\cos\theta_s\sin\theta_s+2D_{xy}^c(\cos\theta_n\sin\theta_s+\sin\theta_n\cos\theta_s+D_{yy}^c\sin\theta_n\cos\theta_n$$

where in Eq.(11), D_{xx}^c,$D_{xy}^c$and D_{yy}^cwere derived as follows

$$D_{xx}^c=\rho\gamma^2U_sU_sh\left[-\eta_0(\ln\eta_0)^2-\eta_0+1\right] \quad (12a)$$

$$D_{xy}^c=1.75\rho\gamma\frac{h^2}{r}U_sU_s(1-\eta_0)(2\eta_0\ln\eta_0+\eta_0+1) \quad (12b)$$

$$D_{yy}^{c} = 49.0\rho\frac{h^3}{r^2}U_s U_s\left(-\frac{\eta_0^3}{3}+\frac{\eta_0^2}{2}-\frac{\eta_0}{4}+\frac{1}{12}\right) \quad (12c)$$

In Eqs(12a), (12b) and (12c); z_0=zero bed elevation, U_s=depth averaged velocity in stream-wise direction, h=depth of the flow, $\eta_0 = z_0/h$ r=radius of channelcurvature.

Values of D_{xx},D_{xy} and D_{yy} *from*Eqs(12a),(12b) and (12c) can be used in Eqs(7) and (8) respectively.

4. Numerical solution procedure

The governing equations presented in Section-3.2 are discretized using the finite volume method in curvilinear, non-staggered grid. In the curvilinear co-ordinate system, mass and momentum equation can be written in conservative tensor notation form as[19] [14],

Continuity Equation

$$\frac{\partial(\rho hJ)}{\partial\tau}+\frac{\partial}{\partial\xi^m}(\rho hJ\hat{u}_m)=0 \quad (13)$$

Momentum Equation

$$\frac{\partial(\rho hJU_i)}{\partial\tau}+\frac{\partial}{\partial\xi^m}\left(\rho hJ\hat{u}_m U_i-\Gamma hJ\alpha_j^m\alpha_j^m\frac{\partial U_i}{\partial\xi_m}\right) \quad (14)$$

$$=-\frac{\partial}{\partial\xi_m}(\rho ghJ\alpha_j^m H)+JS_{u_i}$$

In Eqs(13) and (14); $\hat{u}_m$ (m=1, 2) are the velocity components in the curvilinear coordinate (ξ, η, τ) which relates to U_x, U_y and others as follows, where $\alpha_i^m = \partial\xi_m/\partial x_i$

$$\begin{pmatrix}\hat{u}_\xi\\ \hat{u}_\eta\end{pmatrix}=\begin{pmatrix}\alpha_1^1 & \alpha_2^1\\ \alpha_1^2 & \alpha_2^2\end{pmatrix}\begin{pmatrix}U_x\\ U_y\end{pmatrix}=\begin{pmatrix}\xi_x & \xi_y\\ \eta_x & \eta_y\end{pmatrix}\begin{pmatrix}U_x\\ U_y\end{pmatrix} \quad (15)$$

In Eq.(14), $\Gamma=\rho\nu_t$ = diffusitivity;

$U_i$stands for depth averaged velocities (i=x, y), S_{ui} is the corresponding source term in the equation for U_i, J is the *Jacobian* of transformation between Cartesian coordinate system x_i (x_1=x, x_2=y) and the computational curvilinear coordinate system ξ_m (ξ_1=ξ and ξ_2=η)

Source terms includes cross derivative diffusive terms, dispersion stress terms and external forces but excludes the second derivatives of coordinates (curvature terms) that are very sensitive to grid smoothness [14].

The computational domain is discretized into finite number of control volumes by a computational body fitted grid. The gridlines are identified as cell faces. The control volume centered at point P is embraced by four faces *w, s, e* and *n* (See Fig.3). It is connected with four adjacent control volumes centered at points *W, E, S* and *N*. Here, W denotes west (the negative ξ direction) *E* the east (positive ξ direction), *S* the south (negative η direction) and *N* the north (positive η direction). The convection terms in Eq. (2) are discretized by Hybrid Linear/Parabolic Approximation (HLPA) scheme [18]. The HLPA scheme is reported to be good at stability and accuracy [14]. The diffusion terms are discretized by central difference scheme. The time derivative term is discretized by first order backward scheme.

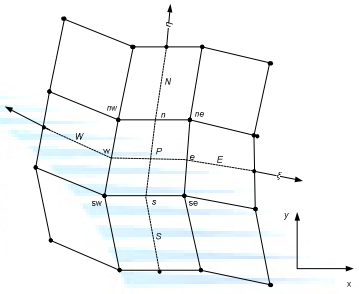

Fig.3Control volume set up

Integrating the transport equation (Eq.14) over the control volume shown in Fig. 3, the resulting descritized equations can be written as[19],

$$U_{i,P}^{*}=\alpha_u\left[\frac{1}{a_P'^{U_i}}\left(\sum_{l=N,S,E,W}a_l U_{il}^{*}+S_{U_i}^{*}\right)+\tilde{D}_i^{1}\left(H_w^{*}-H_e^{*}\right)+\tilde{D}_i^{2}\left(H_s^{*}-H_n^{*}\right)\right]+(1-\alpha_u)U_{i,P}^{o} \quad (16)$$

where $\tilde{D}_i^m = D_i^m\Big/\left(1-\alpha_u\sum_{l=E,W,N,S}a_l^U/a_P^U\right)$ and

$$D_i^m=\frac{(\rho ghJ\,\alpha_i^m\Delta\xi^m)_P}{a_P'}$$

In Eq. (16) $a_P'^{U_i}$, a_l, $\tilde{D}_i^m$ are the coefficients of discretized equations and $U_{i,l}^{*}$, α_u, $U_{i,P}^{o}$, and $S_{U_i}^{*}$ are guessed velocities, under-relaxation factor (taken as=0.8), old values of velocities and source term respectively. H^*_w, H^*_e, H^*_s andH^*_n are guessed water surface level at cell faces of the control volume centered at *P*.

Similarly, integrating the continuity equation (Eq.13) over the control volume, resulting equation can finally be obtained in terms of pressure correction equation as

$$a_P^p H_P' = a_W^p H_W' + a_E^p H_E' + a_S^p H_S' + a_N^p H_N' + S_P \quad (17)$$

In Eq.(17), a_P^p, a_W^p, a_E^p, a_N^p, a_S^p are the coefficients in discretized equation and H' with *P, W, E, N, S* subscripts denote pressure corrections; S_p is the source term of pressure correction equation. H' is related to updated *H* and guessed *H* by following relation (Eq.18).

$$H^{k+1} = H^{*} + H' \quad (18)$$

$$U_{i,P}^{k+1} = U_{i,P}^{*} + \alpha_u \left[\tilde{D}_i^1 (H'_w - H'_e) + \tilde{D}_i^2 (H'_s - H'_n)\right] \quad (19)$$

Velocities are then updated by Eq.(19) by evaluating pressure corrections at cell faces of the control volume centered at *P*. *k* superscript denotes the time step number. The discretized equations are solved through well-known iterative Alternating Direction Implicit (ADI) scheme. To avoid the problem of spurious numerical oscillation, the momentum interpolation technique proposed by Rhie and Chow[13] is used to evaluate the cell face variables from centered quantities and Semi- Implicit Method for Pressure Linked Equations-Consistent (SIMPLEC) algorithm is then established as above to solve the governing equations [8][14].

4.1 Special treatment of the source term in momentum equations

Source term is linearized in the momentum transport equation and includes cross derivative terms and pressure variation terms. In addition, dispersion term is also included in source term (Eq. 8) and integrated over control volume (Fig. 3) to incorporate the effect of dispersion in flow [19].

$$S_{dx} = \iint_{\Delta A} J\alpha_1^1 \frac{\partial D_{xx}}{\partial \xi} + J\alpha_1^2 \frac{\partial D_{xx}}{\partial \eta} + J\alpha_2^1 \frac{\partial D_{xy}}{\partial \xi} + J\alpha_2^2 \frac{\partial D_{xy}}{\partial \eta}$$

$$S_{dy} = \iint_{\Delta A} J\alpha_1^1 \frac{\partial D_{xy}}{\partial \xi} + J\alpha_1^2 \frac{\partial D_{xy}}{\partial \eta} + J\alpha_2^1 \frac{\partial D_{yy}}{\partial \xi} + J\alpha_2^2 \frac{\partial D_{yy}}{\partial \eta} \quad (20)$$

In Eq. (20), S_{dx} and S_{dy} are source terms for dispersion stress contribution in first and second momentum equations respectively.

4.2 Boundary implementation

Velocities at wall boundary is assumed to be non-slip and assigned zero. Near wall boundary, wall function approach is employed. The resultant wall shear stress $\vec{\tau}_w$ is related to flow velocity $\vec{U}_P$ at the center *P* of the control volume close to wall as follows [14]

$$\vec{\tau}_w = -\lambda_w \vec{U}_P \quad (21)$$

For evaluating λ_w [14] may be referred. The pressure (water level) at South(*S*) and North (*N*) boundary points can be extrapolated from values at adjacent internal points. Since the wall velocity is known, it is also unnecessary to perform a pressure correction here. Discharge is specified at the inlet boundary and water level is specified at the outlet downstream boundary. Flow velocity at the outlet can be extrapolated from the values at the adjacent internal points. Flux correction and pressure correction is kept zero respectively at the outlet and inlet boundaries.

4.3 Computation of bed friction coefficient

Using uncertainty approach it is established that, over a non-uniform river reach *U* is likely to have far greater spatial variability than *n,* so will be the dominant control over spatial variation in shear stress [3]. Physically based alternative to estimate n, is used as mentioned in the following equation [3]. The assumption considered is that law of wall holds throughout the full depth to estimate value of C_D at each node.

$$n = \frac{\kappa h^{\frac{1}{6}}}{\sqrt{g}\ln\left(\frac{h}{e \cdot z_0}\right)} \quad (22)$$

z_0 (Roughness height) $= \frac{\kappa_s}{30}$ or more recently $= 0.1 D_{84}$, *h*=flow depth, *e*=2.71.

4.4 Wetting and drying technique

In open channels with sloped banks, sand bars, and islands, the water edges change with time, and some part of the domain might be dry. A number of methods have been reported in the literature to handle this problem. The 'fixed grid' that covers the largest wet domain (Primary flood plain) and treats dry nodes as part of the solution domain is used [14]. It includes the "small imaginary depth," method. The "small imaginary depth" method uses a threshold flow depth (a low value, such as 0.02m in natural rivers and 0.001m in experimental flumes) to judge drying and wetting at each time step. The dry nodes are assigned zero velocity. The water edges between the dry and wet areas can be treated as internal boundaries, at which the wall-function approach was applied. The dry nodes can be excluded from the computation in an explicit algorithm, but must usually be included in an implicit algorithm.

5. Simulation results and discussion

One of the main advantages of Brahmaputra River is that it has three to four constrict nodal points where the cross-sections remain unaltered and stable with time and space, moreover, around the vicinity within an extent, Brahmaputra follows uniform aligned channel configuration. This gives different segments of Brahmaputra separated with well-defined nodal points

(with uniform channel width) which is favorably suited for applying 2-D hydrodynamic mathematical model as far as upstream and downstream boundary implementation is concerned. Still, process representation of fully developed braided stream is challenging due to the presence of numerous 3-D flow structures within the flow domain. Second advantage that, the river Brahmaputra is one of the rivers which are well under the observation of different stake holders. The importance of the information that could be derived from the analysis of the data is very high in the design, management and future risk and hazard strategies. More the data sets better is the result's reliability. The study has been carried out for the study domain of the river channel (from Pandu to Jogighopa) - (Approx. 100 km) with 14 numbers of measured river cross sections (1997) and hydrological Data (Jogighopa-Pandu) for the same year.

The flow in long reaches of river is 3-D dimensional and essentially an unsteady flow. To simulate 2-D flow for such a long reach with width varying from 2km to 22km is heavily data intensive. Practically, data required for simulating unsteady flow in 2-D are hard to acquire for such a large alluvial river like the Brahmaputra. Yet for practical engineering purposes, steady flow simulation using 2-D model for large alluvial river provides desirable information and enough insight to approximate realistic flow situation.

The generated flow domain (low flood plain and main channel) from Satellite imagery and constructed mesh is presented again in Fig.(4a). The bed elevation profile was generated using the measured cross-sectional data at predefined locations through interpolating the bed through application of Nearest Neighbourhood Method using Matlab code (shown in Fig.(4b)).

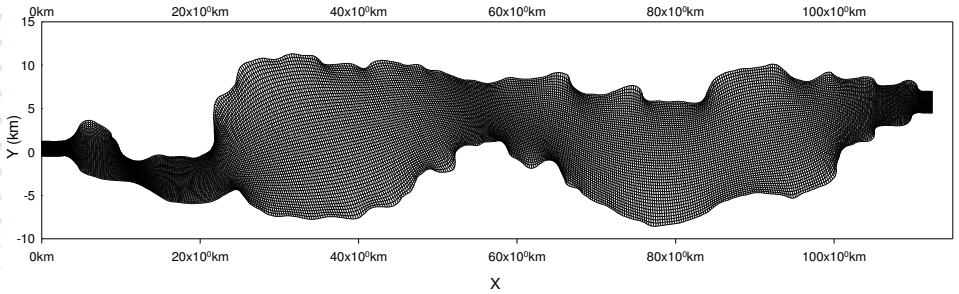

Fig.4a Generated mesh for Brahmaputra study reach

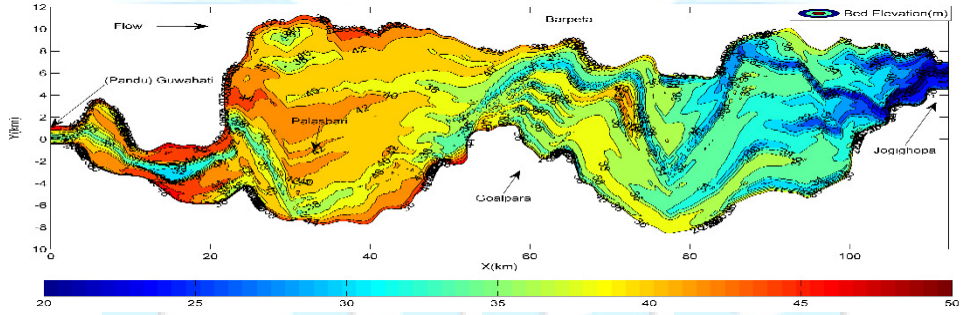

Fig. 4b. Bed elevation profile for Brahmaputra study reach for 1997

5.1 Model validation

Model verification was done with comparing measured water stages at Pandu site with model simulated water stages. Measured stages at downstream Jogighopa were implemented as downstream boundary condition. Observed discharges were assigned at Pandu as upstream boundary condition and discharge at the downstream boundary were computed from model results as simulated discharges for comparison. 2-D flow model was used for 20 discharge *profiles* (designated as *profile*-1 to *profile*-20 respectively) for receding flood of 1997 (12th July 1997 to 31st July 1997) and validation results are presented in Fig. 5 and Table 1. It can be seen that the simulated stages are in fair agreement with the measured. Amongst the hydrological data, water level can be considered to be the most reliable primary data with minimum error in comparison to other data. In the above context, the good

reproduction of stages is quite encouraging for the enhanced 2-D depth averaged modelling approach considered, for such a highly braided curvilinear stretch of Brahmaputra River.

5.2 Variation of flow variables

(i)Variation in Water Depth and Water Surface Elevation

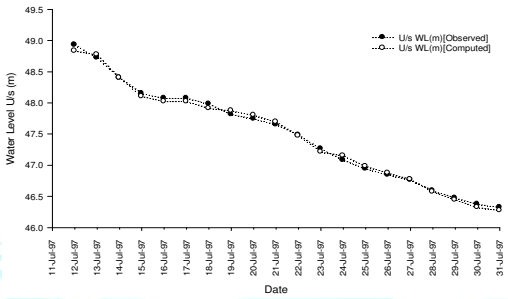

Fig. 5 ObservedWSL verses computed WSL plot at Pandu (end node)

The contour plot of model simulated water depth for discharge *profile*s 1, 3, 16 and 20 have been shown in Fig.(6). One can observe that with decreasing discharges into the flow domain, from *profile*-1 to *profile*-20, flow area shrinks around the deepest bed level with increasing no flow zone or zones with shallow water depths. Highest water depth is around 12-10 m found in the inlet and outlet of the flow domain where river constricts to narrow with incised configurations. Water depths across the river are as low as 2 m where the river fans out at Palasbari (20 km to 40 km from the inlet at Pandu). Such a large variation of water depth along the thalweg (Deepest bed level) is one of the special features of Brahmaputra River. This special character due to typical bed geometry of the river at a particular instance of time induces a very high dissipation of flow energy to the bank-lines through evolution and diminishing of secondary flow field. High dissipation of flow energy makes bank-lines vulnerable to severe river bank erosion.

Table 1. Comparison between measured water stages and discharges at upstream and downstream locations respectively for designated discharge *profile*s.

Discharge Profiles	Date	Observed WL(m)	Computed WL(m)	Actual Discharge (Cumecs)	Computed Discharge (Cumecs)	Absolute Error in WL (cm)
1	12-Jul-97	48.93	48.83	49389.69	49241.40	10.00
2	13-Jul-97	48.72	48.77	46269.77	46141.35	5.00
3	14-Jul-97	48.4	48.4	41866.74	41769.65	0.00
4	15-Jul-97	48.15	48.1	38725.74	38616.61	5.00
5	16-Jul-97	48.07	48.02	37854.29	37753.99	5.00
6	17-Jul-97	48.07	48.02	37834.47	37692.20	5.00
7	18-Jul-97	47.98	47.91	36788.31	36697.66	7.00
8	19-Jul-97	47.81	47.87	34808.59	34691.10	6.00
9	20-Jul-97	47.74	47.8	34119.5	34055.45	6.00
10	21-Jul-97	47.65	47.69	33153.9	33077.78	4.00

11	22-Jul-97	47.48	47.47	31330.32	31240.26	1.00
12	23-Jul-97	47.26	47.21	29289.57	29213.12	5.00
13	24-Jul-97	47.08	47.15	27649.36	27570.90	7.00
14	25-Jul-97	46.94	46.98	26419.21	26357.51	4.00
15	26-Jul-97	46.84	46.87	25590.78	25552.40	3.00
16	27-Jul-97	46.76	46.77	24936.58	24912.53	1.00
17	28-Jul-97	46.59	46.57	23547.83	23530.02	2.00
18	29-Jul-97	46.47	46.44	22663.52	22650.32	3.00
19	30-Jul-97	46.37	46.32	21920.12	21893.58	5.00
20	31-Jul-97	46.32	46.27	21562.88	21541.23	5.00

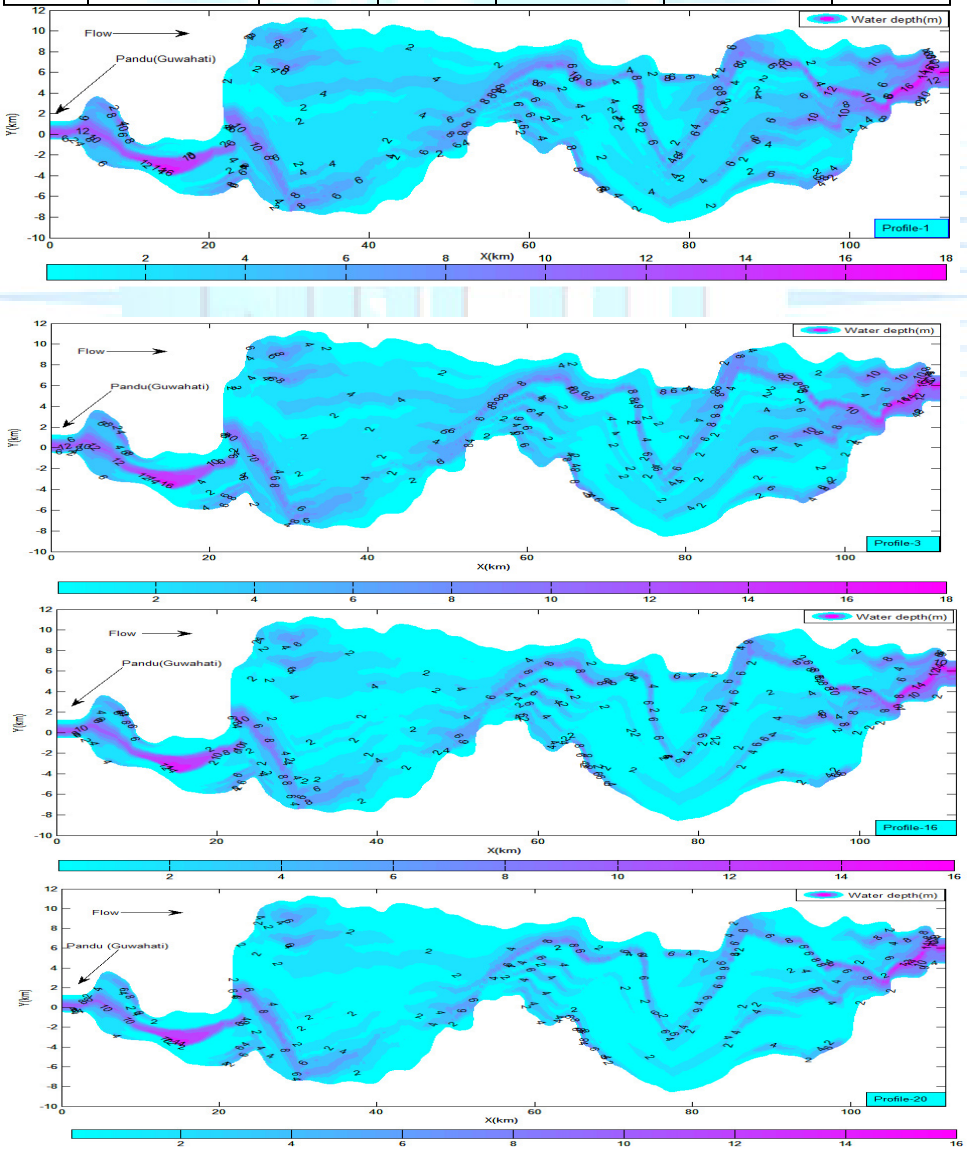

Fig. 6 Contour-plot for water depth for*dischargeprofile*s 1, 3, 16 and 20 (see Table 1)

Contours for water surface elevation (WSL) for the same *profiles* i.e. 1, 3, 16 and 20 are presented in Fig. (7). Implementing the wetting and drying technique, the dry zones in the flow domain were simulated for different discharge *profiles*. The dry zones with zero water depth have been shown in black shades in Fig. (7), for simulated discharge *profiles* namely 1, 3, 16 and 20. At channel bifurcations, although flow-fields are essentially three dimensional, yet braid bars or side bars (simulated dry zones) were approximated with reasonable accuracy using the developed enhanced model through implementing wetting and drying technique without developing numerically more expensive 3-D model for such macro-scale flow field scenario. Looking at the Fig. (7), it was observed that braiding intensity was increasing with decreasing discharges, more and more braid bars and side bars were evolved, thereby increasing the proportionate no flow zone in the flow domain.

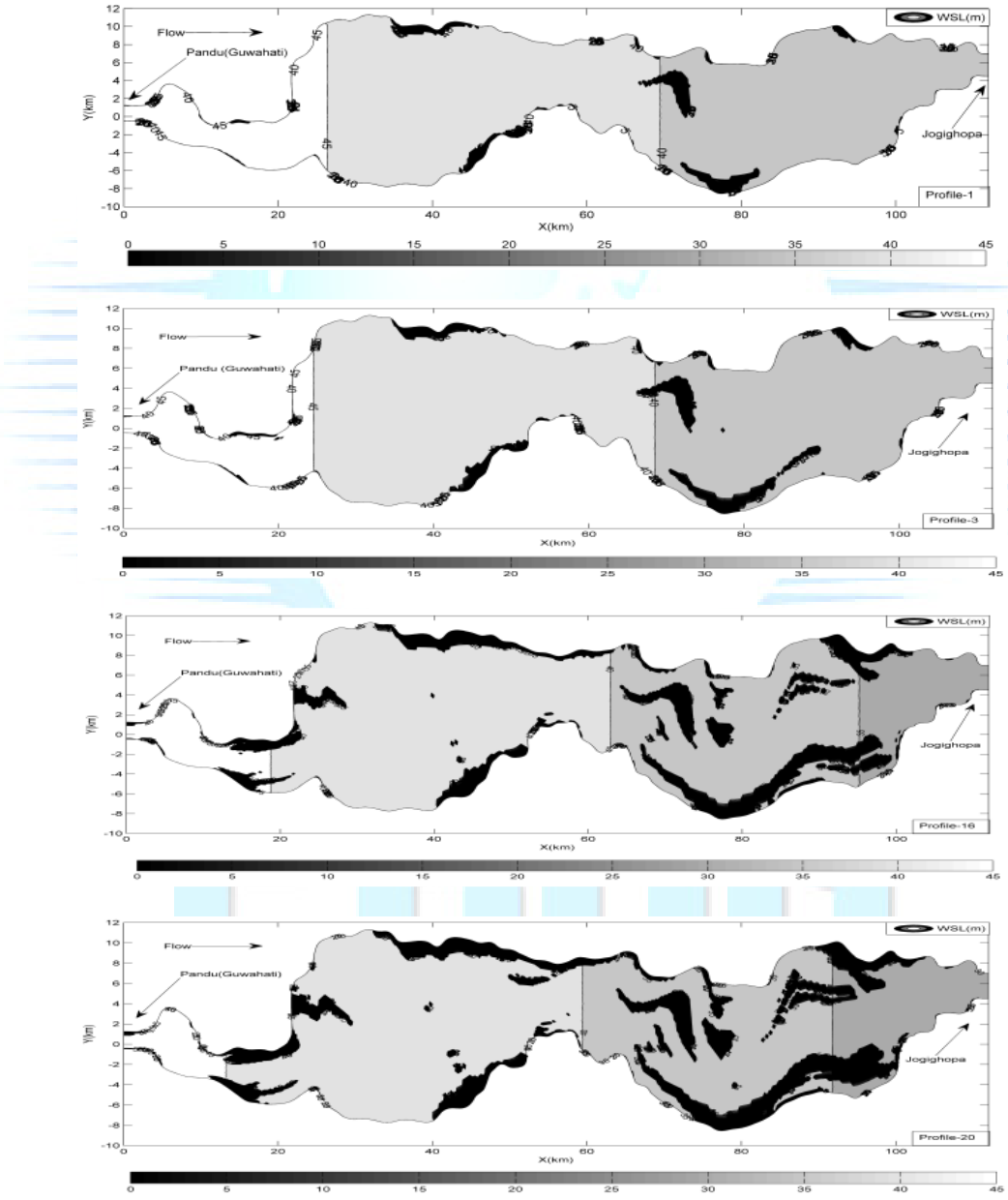

Fig.7Contour-plot for water surface level (WSL)ford*ischarge profiles* 1, 3, 13, 16 and 20

(ii) Variation in Flow Field

Simulated stream-wise velocity vector plots for the study flow domain are presented in Fig. 8 for discharge *profile*s 3, 16 1nd 20 for illustrating decreasing concentration of flow with decreasing discharges. Figures 9a, 9b, 9c, 9d, 9e and 9f are shown here to illustrate the simulated velocities at some important specific locations for *profile*-1. Figures (9a) and (9b) are shown to depict the streamwise velocity vector near Goalpara Town (40 to 80 km downstream of Guwahati). Variation of stream-wise velocity along the bank-line of Brahmaputra River in upstream location of Golapara Town is shown in Fig. 9c and in downstream location of Goalpara Town in Fig. 9d. The important location chosen was near Guwahati (0 km to 25 km from inlet location at Pandu). At Pandu (Guwahati), river is incised and stable with rock out-crops. Figure 9c shows the velocity *profile* from 0 to 10 km from Guwahati where River is narrow and velocity is high. In Fig. 9d velocity vector plot is shown for the location 12-25km from Guwahati, from where river width starts widening almost to 20 km at Palasbari. Similarly Figs 9e and 9f are presented to depict the transverse velocity field near Guwahati and Goalpara Town.

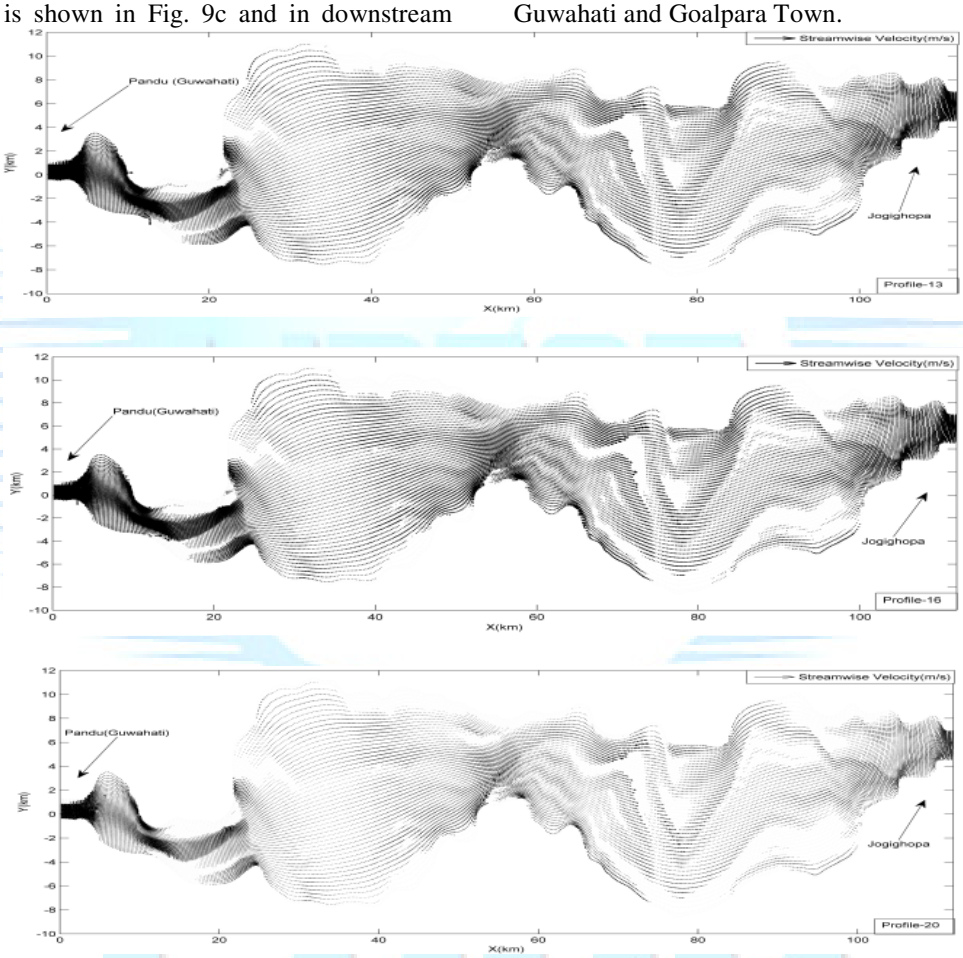

Fig 8 Vector-plot for stream-wise velocity for*discharge profiles* 13, 16 and 20

From the figure, it was observed that concentrations of high velocities are confined to certain specific flow regions. These locations are at the inlet of the flow domain near Guwahati (stream-wise velocity almost 3.5 m/s at discharge Profile-1, location- x=0-5 km, y=0), at 55km downstream of Guwahati near Goalpara Town (stream-wise velocity is 2.5m/s at Profile-1; location- x= 52-58 km, y=0-4 km), at 65 to 75 km (location: x=65-75km, y=8 to -6 km) and at the outlet at Jogighopa (x=112 km, y=4-7km) . In this simulated flow field these locations do not change due to rigid bed consideration in the developed model. Apart from these locations, magnitude of the velocity in the flow-field is lowered down almost to 0.5 m/s.

7. New Braiding Indicator based on model results.

Contour plots shown in Fig. 7 are further analyzed. Simulated dry cell nodes (where water depth was zero) for

each *profile* were identified and sum of the area of drycells for each *profile* simulation was evaluated. Thus, area of no flow zone is calculated for each simulated *profile*.

Dividing it by total area of flow domain, fractional no flow ratio (f_{nf}) was calculated. No flow area was subtracted from total flow area and fractional flow ratio (f_f) was estimated. Simulated fractional flow ratio and no flow ratio(f_{nf}) for*profile* 1 to 20 were tabulated in Table 2. It was observed that with decreasing discharges, no flow ratio decreases. The rate of decrease of no flow ratio with observed discharge also depends upon the geometric configuration of the flow domain along with other factors. Based on the obtained results and information from flow simulation for twenty discharge *profiles* at receding flood of 1997, an indicator namely *braid power* is proposed based on the model output to express the measure of braiding for a river reach as follows.

$$braid\ power(\mathrm{N/m^2\text{-}s}) = f_{nf} \cdot \frac{\gamma Q_{inlet} S}{\text{flow Area of Inlet of the Reach}} \quad (24)$$

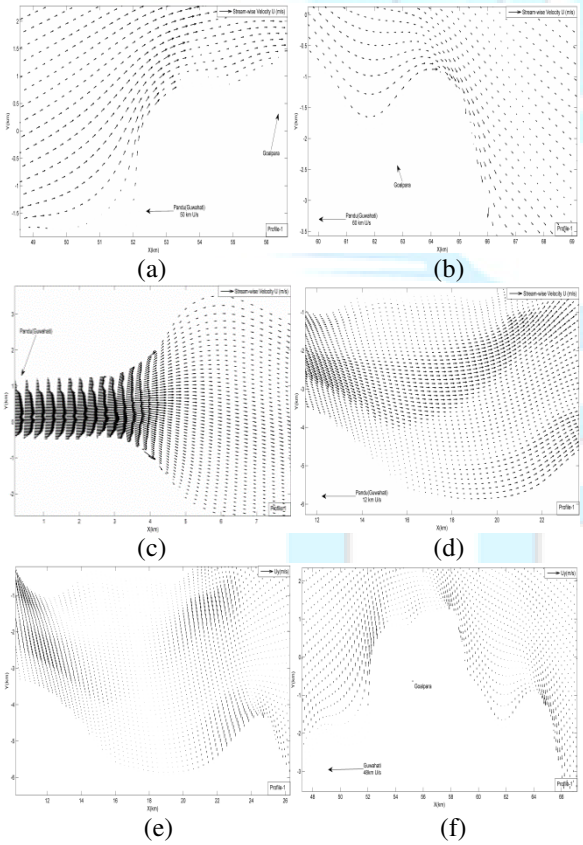

Fig.9Vector-plot for U and U_y at selected locations for *profile*-1

Moreover, flow field shrinks around the thalweg (deepest bed level) with decreasing discharges.

6. Variations of longitudinal velocity deviation intensities

Longitudinal velocity deviation intensity (I_L) and transverse velocity deviation intensity (I_T) give the fractional deviations of discrepancy with respect to depth averaged velocity in stream-wise and transverse direction [14].

$$I_L = \left(\frac{\frac{1}{h}\int_0^h u_\xi'^2 dz}{U^2} \right) \quad (22)$$

$$I_T = \left(\frac{\frac{1}{h}\int_0^h u_\eta'^2 dz}{U^2} \right) \quad (23)$$

In Eqs(21) and (22); u_ξ' and u_η' =longitudinal and transverse velocity deviations with respect to depth averaged velocities, u_ξ and u_η in ξ and η direction respectively. While conducting flow simulation for the Brahmaputra River Stretch, I_L and I_T were computed for all discharge *profiles*. For further analysis, stream-wise deviation $I_L$was chosen to see its variations along the river stretch under study. *Mean*I_L was obtained through averaging I_L for all cell centers lying at each transverse η-line in the study domain. Thereafter, it was plotted against longitudinal distances from inlet to outlet locations for *Discharge profiles* 1, 3, 6, 9, 13, 16 and 20 (Fig. 11). Spatial variations of I_L helped to identify the meandering behavior of the braided river. It increases rapidly wherever stream has well developed curved flow domain (Fig. 11). As the discharge, decreases (*profile*-1 to 20), *mean* $I_L$along the reach has more fluctuations with increased numbers of peak values. It indicates that as the discharge decreases, dispersion is more predominant. In other words, when intensity of braiding increases, it evolves multiple channels with meandering configurations. Meandering and bend in evolved multiple channels instigate more discrepancy in the flow-field if it is approximated with depth averaging. Hence, velocity deviations intensities are more prominent at low discharges. Hence, at lower discharges with high braiding, dispersion stress terms are

well justified to include into the flow model for better assessment of the flow field.

For a given river reach, when f_{nf}approaches 1, Q_{inlet}approaches zero,at the same time Flow area at inlet also approaches zero. *Braid power* becomes very large and approaches infinity.

Similarly, when f_{nf}approaches zero, *braid power* approaches zero (Eq. 24).Within the range of f_{nf}between 0-1, *braid power* is nothing but a fraction of unit stream power per unit depth of flow at the inlet location of reach under consideration.The reported average longitudinal slope of the study reach is 0.11m/km [2]. Hence, *braid power* was computed for twenty simulated discharge profiles and braid power verses observed discharge was plotted and shown in Fig. 12 (Table 2).

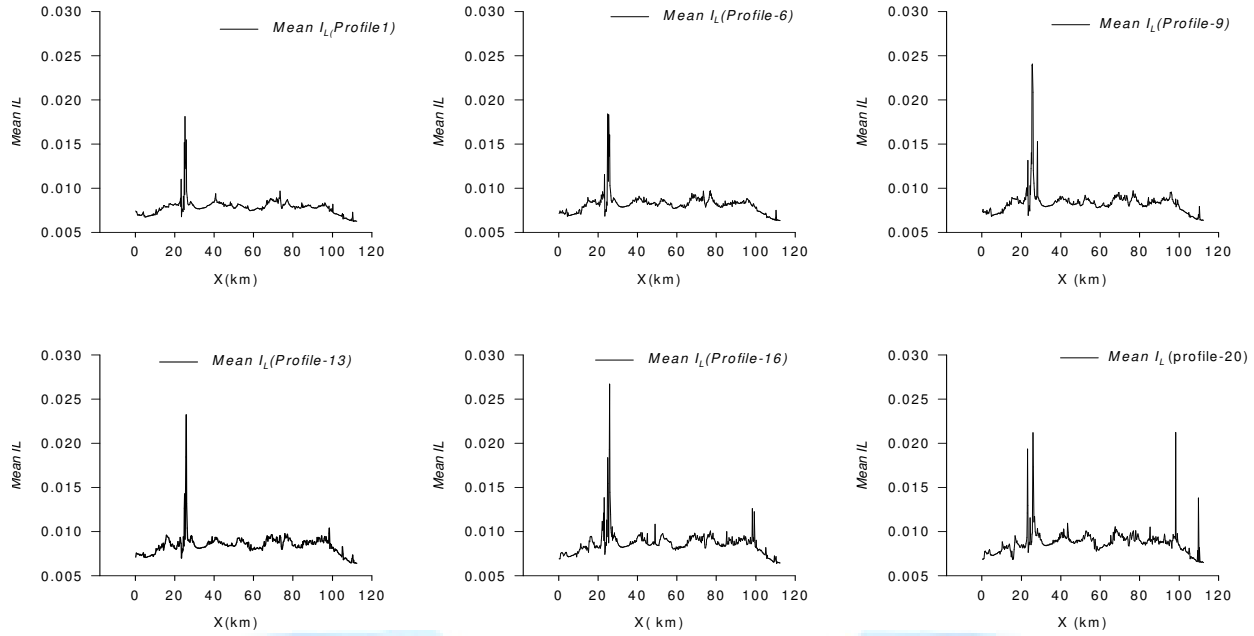

Fig. 11 Mean *l*ongitudinal velocity deviations (I_L) for *profiles* 1, 6, 9 13 16and 20

Table 2. Model simulated computation of no flow zone and estimation of *braid power*

Discharge profiles	Date	Fractional Flow Ratio (simulated)	No Flow Ratio (Simulated)	Braid Power (N/m^2-s)
1	12-Jul-97	0.9703	0.0297	0.110
2	13-Jul-97	0.9684	0.0316	0.111
3	14-Jul-97	0.9581	0.0419	0.139
4	15-Jul-97	0.9493	0.0507	0.161
5	16-Jul-97	0.9462	0.0538	0.168
6	17-Jul-97	0.9461	0.0539	0.168
7	18-Jul-97	0.9451	0.0549	0.169
8	19-Jul-97	0.9384	0.0616	0.180
9	20-Jul-97	0.9352	0.0648	0.187
10	21-Jul-97	0.9298	0.0702	0.200
11	22-Jul-97	0.9173	0.0827	0.228
12	23-Jul-97	0.9042	0.0958	0.254
13	24-Jul-97	0.8979	0.1021	0.258
14	25-Jul-97	0.8867	0.1133	0.278
15	26-Jul-97	0.8797	0.1203	0.290
16	27-Jul-97	0.8739	0.1261	0.299
17	28-Jul-97	0.8606	0.1394	0.320
18	29-Jul-97	0.8503	0.1497	0.336
19	30-Jul-97	0.8398	0.1602	0.352
20	31-Jul-97	0.836	0.164	0.357

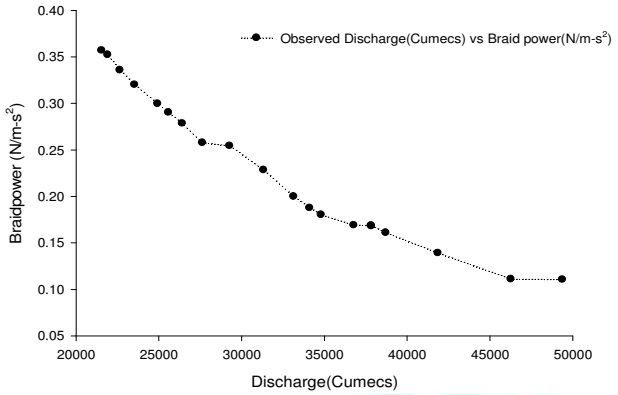

Fig. 12 Plot for observed discharge vs. *braid power* for the study reach

It was observed that *braid power* increases with decrease in incoming discharge into the reach at a particular instance of time (Fig. 12). The rate of decrease or increase of *braid power* depends upon geometric configuration of the reach at the particular instance of time along with other factors.

6. Conclusions

In this study, two dimensional enhanced numerical model with boundary fitted coordinate system and secondary flow corrections for the Brahmaputra River Stretch with highly braided configuration, has been developed and verified.

1. It has been observed that effect of dispersion stress tensor in flow field increases with increase in braiding intensity. Model results shown, adequately support this statement. When intensity in braiding increases, it evolves multiplechannels with meandering configurations. Meandering and bend in evolved multiple channels instigate more discrepancy in the flow-field if it is approximated with depth averaging.

2. Realistic assessment of predictions of bank erosion and river bed evolution for braided alluvial rivers is expected with Improved and realistic flow-field estimation with secondary flow correction as the prime input.

3. A simplified indicator namely braid power for measuring intensity of braiding for a given river reach is evolved based on the model results. It was observed that braid power increases with decrease in incoming discharge into the reach at a particular instance of time

Acknowledgement

Some specific field data used in the present study was supplied by National Disaster Management Authority of India (NDMA, Govt. of India), New Delhi, which is gratefully acknowledged here.

Notations

B=channel width;C_d=frictional stress coefficient; D^c_{xx}, D^c_{xy}andD^c_{yy}=components of dispersion coefficient tensor in curvilinear coordinates;D_{xx}, D_{xy}andD_{yy}=components of dispersion coefficient tensor in Cartesian coordinates; g =acceleration of gravity;H =water surface elevation;h=flow depth;I_L = non-dimensionallized values of the longitudinal velocity deviation;I_T=non-dimensionallized values of the transverse velocity deviation;J=Jacobian; k_s =roughness height;n=Manning's coefficient;ξ =stream-wise direction;η=transverse direction;κ =*Von Karman's* constant;v_t =eddy viscosity;Γ =diffusivity;ρ =density of flow;t =time; $\hat{u}_m$ =depth averaged velocity in curvilinear coordinate system;U =stream-wise depth averaged velocity;U_x, U_y=depth averaged velocities in Cartesian coordinates;x, y = Cartesian coordinate;z =vertical coordinate;z_0 =zero velocity level;

References

[1] WAPCOS, "Morphological studies of river Brahmaputra", New Delhi, 1993.(17)
[2] Sarma J. N. "Fluvial process and morphology of the Brahmaputra River in Assam, India", Science Direct, Geomorphology, Vol. 70, No. 2005, pp.226– 256(13)
[3] Bates P.D., Lane S.N. and Ferguson R.I. (2005). "Computational Fluid Dynamics, Applications in Environmental Hydraulics" United Kingdom: John Wiley and Sons, Ltd, 2005.
[4] Prandtl, L. (1952). "Essentials of fluid dynamics", London, Blackie and Sons Press Trust of India Report, (1995), The Sentinel, 7th July, pp. 3, 1952
[5] Lien, H. C., Hsieh, T. Y., Yang, J. C., and Yeh, K. C., "Bend flow simulation using 2D depth-averaged model." J. Hydraul. Eng., Vol.125, No.10, 1999, pp. 1097–1108.
[6] Smith, N.D., "The Braided Stream Depositional Environment", Comparison of the Platte river with some Silurian Clastic Rocks, North central Appalacfians, Geological Society of America Bulletin,.Vol. 81, 1970, pp. 2993-3014.
[7] Sankhua, R.N. "ANN based spatio-temporal morphological model of the river Brahmaputra." PhD Thesis, Dept. of WRD&M, I.I.T. Roorkee, 2005.
[8] Majumdar, S.,Rodi, W. and Zhu, J. "Three-dimensional finite-volume method for incompressible flows with complex boundaries." J.Fluids Eng., Vol. 114, 1992, pp. 496-503.
[9] Odgaard, A. "River meander model. I: Development." J. Hydraul. Eng., Vol.115, No.11, 1989a, pp. 1433–1450.
[10] Seo, Won, Lee, MyungEun., and Baek, Kyong Oh "2D modeling of heterogeneous dispersion in meandering

channels." J. Hydraul. Eng., Vol. 134, No. 2, 2008. pp. 196-204.

[11] Rhie, T.M. and Chow, A. (1983). "Numerical study of the turbulent flow past an isolated air foil with trailing –edge separation." AIAA J., Vol.21, 1983, pp.1525-1532.

[12] Sharma, Nayan, "Mathematical Modelling and Braid Indicators." In The Brahmaputra Basin Water Resources, V.P.Singh (Ed.), Dordrecht: Kluwer Academic Publishers, Vol. 47, 2004, pp. 229-260.

[13] Rhie, T.M. and Chow, A. (1983). "Numerical study of the turbulent flow past an isolated air foil with trailing –edge separation." AIAA J., Vol.21, 1983, pp.1525-1532.

[14] Wu Weiming "Computational River Dynamics." UK: Francis Group, London,, ISBN 978-0-415-44961-8, 2007

[15] Duan, J. G. and Pierre Y. Julien, Y. P. "Numerical simulation of the inception of channel Meandering'." Earth Surf. Process. Landforms Vol.30, 2005, pp.1093–1110.

[16] Duan, Jennifer G. "Simulation of flow and mass dispersion in meandering channels." J Hydraulic. Eng., Vol. 130, No.10, 2004, pp. 964-976.

[17] Kalkwijk, J. P. T., and de Vriend, H. J. "Computation of the flow in Shallow River bends". J. Hydr. Res., Vol. 18, No. 4, 1980, pp.327-342.

[18] Zhu, J. and Rodi, W. (1991). "A low dispersion and bounded convection scheme." Comput. Meths. Appl. Mech. Eng., Vol. 92, 1991, pp. 87-96.

[19] Akhtar, M.P., Sharma Nayan, Ojha, C.S.P. and Bergstrom, D.J. "A Numerical Study of Flow Dispersion Stresses in 2D Depth Averaged Model for Curvilinear Flow Domain" Int. Jr. of Scientific Engineering and Technology, Vol. 3, No. 7, 2014,pp.925-929.